

Liquid Fluoride Salt Experiment Using a Small Natural Circulation Cell



**Approved for public release;
distribution is unlimited.**

Graydon L. Yoder, Jr.
Dennis Heatherly
David Williams
Oak Ridge National Laboratory

Josip Caja
Mario Caja
Electrochemical Systems, Inc.,

Yousri Elkassabgi
John Jordan
Roberto Salinas
Texas A&M University

April 2014

DOCUMENT AVAILABILITY

Reports produced after January 1, 1996, are generally available free via US Department of Energy (DOE) SciTech Connect.

Website <http://www.osti.gov/scitech/>

Reports produced before January 1, 1996, may be purchased by members of the public from the following source:

National Technical Information Service
5285 Port Royal Road
Springfield, VA 22161
Telephone 703-605-6000 (1-800-553-6847)
TDD 703-487-4639
Fax 703-605-6900
E-mail info@ntis.gov
Website <http://www.ntis.gov/help/ordermethods.aspx>

Reports are available to DOE employees, DOE contractors, Energy Technology Data Exchange representatives, and International Nuclear Information System representatives from the following source:

Office of Scientific and Technical Information
PO Box 62
Oak Ridge, TN 37831
Telephone 865-576-8401
Fax 865-576-5728
E-mail reports@osti.gov
Website <http://www.osti.gov/contact.html>

This report was prepared as an account of work sponsored by an agency of the United States Government. Neither the United States Government nor any agency thereof, nor any of their employees, makes any warranty, express or implied, or assumes any legal liability or responsibility for the accuracy, completeness, or usefulness of any information, apparatus, product, or process disclosed, or represents that its use would not infringe privately owned rights. Reference herein to any specific commercial product, process, or service by trade name, trademark, manufacturer, or otherwise, does not necessarily constitute or imply its endorsement, recommendation, or favoring by the United States Government or any agency thereof. The views and opinions of authors expressed herein do not necessarily state or reflect those of the United States Government or any agency thereof.

Reactor and Nuclear Systems Division

LIQUID FLUORIDE SALT EXPERIMENT USING A SMALL NATURAL CIRCULATION CELL

Graydon L. Yoder, Jr.

Dennis Heatherly

David Williams

Oak Ridge National Laboratory

Josip Caja

Mario Caja

Electrochemical Systems, Inc., Knoxville, Tennessee

Yousri Elkassabgi

John Jordan

Roberto Salinas

Texas A&M University, Kingsville, Kingsville, Texas

April 2014

Prepared by

OAK RIDGE NATIONAL LABORATORY

Oak Ridge, Tennessee 37831-6283

managed by

UT-BATTELLE, LLC

for the

US DEPARTMENT OF ENERGY

under contract DE-AC05-00OR22725

CONTENTS

	Page
LIST OF FIGURES	v
LIST OF TABLES	vii
ACRONYMS AND ABBREVIATIONS	ix
NOMENCLATURE	xi
ABSTRACT.....	1
1. INTRODUCTION	1
1.1 BACKGROUND	1
1.2 EXPERIMENT DESIGN.....	4
1.3 VISUALIZATION.....	9
1.4 IR PHOTOGRAPHY	11
1.5 LASER DOPPLER VELOCIMETRY.....	13
1.6 SALT VELOCITY CALCULATIONS	14
1.7 NATURAL CIRCULATION HEAT TRANSFER DATA	16
2. CONCLUSIONS	23
3. REFERENCES	24

LIST OF FIGURES

Figure	Page
Fig. 1. Schematic of liquid salt cell.....	4
Fig. 2. Upper flange of cell.	5
Fig. 3. Improved top flange.....	6
Fig. 4. Modified top flange showing 76 mm gate valve.	7
Fig. 5. Nickel crucible used to contain liquid salt.....	8
Fig. 6. Outer vessel with crucible inside.	8
Fig. 7. Top flange temporarily assembled to vessel.....	8
Fig. 8. Assembly inserted in furnace.....	9
Fig. 9. Salt cell dimensions.	10
Fig. 10. Photo of salt through sapphire window.	11
Fig. 11. Sapphire window showing “fogging” after 1 month of testing.	12
Fig. 12. Transmittance of sapphire window.....	13
Fig. 13. IR image of heater immersed in salt.	13
Fig. 14. Velocity path lines and magnitude as predicted by FLUENT CFD analysis.	15
Fig. 15. Temperature profiles within the melt.....	16
Fig. 16. Heater 1 thermocouple locations.	18
Fig. 17. Heater 2 thermocouple locations.	18
Fig. 18. Heater 3 thermocouple locations.	19
Fig. 19. Thermocouple probe thermocouple locations.....	19
Fig. 20. Heat transfer coefficient data.	22
Fig. 21. Nusselt number data comparison.....	23

LIST OF TABLES

Table	Page
Table 1. Natural circulation heat transfer data from liquid salt cell testing.....	20
Table 2. Calculated values of heat transfer coefficients	21
Table 3. Comparison of Nu equations of the form $Nu = A(Gr_z Pr)^b$	23

ACRONYMS AND ABBREVIATIONS

AHTR	advanced high-temperature reactor
ANP	Aircraft Nuclear Propulsion (program)
ARE	Aircraft Reactor Experiment
BN	boron nitride
CFD	computational fluid dynamics
FHR	fluoride salt-cooled high-temperature reactor
FLiBe	fluoride
FLiNaK	fluoride salt heat transfer
IHTR	innovative high-temperature reactor
IR	infrared
LDV	laser Doppler velocimeter
MSBR	molten salt breeder reactor
MSR	molten salt reactor
MSRE	Molten Salt Reactor Experiment
ORNL	Oak Ridge National Laboratory
PB-AHTR	pebble bed advanced high-temperature reactor
SmAHTR	small advanced high-temperature reactor

NOMENCLATURE

A_s	heater surface area (based on heated length of heater)
β	salt thermal coefficient of volume expansion
C_p	salt specific heat
g	acceleration of gravity (9.8 m/s^2)
Gr_z	Grashof number $g\rho^2\beta z^3(T_h-T_s)/\mu^2$
h_{nc}	natural circulation heat transfer coefficient
i	current
k	salt thermal conductivity
Nu	Nusselt number $h_{nc} z/k$
ρ	salt density
P	heater power= $V \cdot i$
Pr	Prandtl number $\mu C_p/k$
q''	average heater heat flux: P/A_s
q''_{rad}	radiation correction
T_h	heater temperature
T_h	measured local heater temperature
T_s	measured local salt temperature
T_s	salt temperature
μ	salt dynamic viscosity
V	voltage
z	distance from bottom of heater element

ABSTRACT

A small liquid fluoride salt experiment has been constructed and tested to develop experimental techniques for application in liquid fluoride salt systems. There were five major objectives in developing this test apparatus:

1. Allow visual observation of the salt during testing (which involved determining how lighting could be introduced, how pictures could be taken, and what could be seen).
2. Determine if infrared photography can be used to examine components submerged in the salt.
3. Determine if the experimental configuration provides sufficient salt velocity for collection of corrosion data for future experimentation.
4. Quantify natural circulation salt velocities using a laser Doppler velocimeter.
5. Acquire natural circulation heat transfer data in fluoride salt at temperatures up to 700°C.

All of these objectives were successfully met during testing with the exception of the fourth: quantify natural circulation salt velocities using a laser Doppler velocimeter. This paper describes the experiment and experimental techniques used and presents data taken during natural circulation testing.

1. INTRODUCTION

Effective high-temperature thermal energy exchange and delivery at temperatures above 600°C has the potential for significant national impact by reducing both capital and operating costs of energy conversion and transport systems. It is one of the key technologies necessary for efficient hydrogen production and could potentially enhance efficiencies of high-temperature solar systems. Today there are no standard commercially available high-performance heat transfer fluids effective above 600°C. High pressures associated with water and gaseous coolants (such as helium) at elevated temperatures impose limiting design conditions for the materials in most energy systems. Liquid salts offer high-temperature capabilities at low vapor pressures, good heat transport properties, and reasonable costs and are therefore leading candidate fluids for next-generation energy production. The experiment discussed in this paper examined techniques that could potentially be used to help characterize equipment and process variables in fluoride salt systems while also providing natural circulation heat transfer data.

1.1 BACKGROUND

Major interest in fluoride salts as a heat transfer medium was initiated as part of the Aircraft Nuclear Propulsion (ANP) program in the late 1940s. To develop a lightweight nuclear power source that could be used to support long duration aircraft flights, a high-temperature heat transfer medium was needed. The initial design of the aircraft nuclear reactor used liquid sodium as the coolant, combined with a solid fuel. However, because of reactor physics issues with this design, as well as structural concerns over the solid fuel itself, the project eventually turned to the use of a liquid fuel consisting of sodium, zirconium, and uranium fluoride salts. The ANP program lasted for approximately 12 years and included operation of the first molten salt reactor, the Aircraft Reactor Experiment (ARE) at Oak Ridge National Laboratory (ORNL).¹⁻⁴ This reactor operated for nine days in 1954 at a steady outlet temperature of 850°C and at power of up to 2.5 MW. The ANP program officially ended in 1961; however, it was understood early in the ANP program that liquid salt-fueled reactors could potentially serve as commercial power reactors, given the attractive characteristics of fluoride salts.

Investigation into the application of molten salt reactors for civilian power started in the late 1950s. In 1960, the design of a new molten salt-fueled experimental reactor, the Molten Salt

Reactor Experiment (MSRE), was initiated at ORNL to support the development of the commercial version of this reactor. MSRE was fueled with a mixture of uranium, lithium, beryllium, and zirconium fluorides and was constructed of INOR-8 (now Hastelloy-N), a material developed specifically for molten salt application. Using much of the infrastructure developed for the ARE, MSRE went critical in 1965 and was operated for approximately four years. This included six months of continuous operation at up to ~8 MW, demonstrating that the reactor could be operated stably and that the components were reliable. The reactor was also the first ever to operate fueled with ^{233}U . A good summary of the MSRE test program is presented in reference 5.

The molten salt reactor program continued into the early 1970s and was primarily focused on developing the molten salt breeder reactor (MSBR) concept,⁶ developing full-scale reactor designs, and evaluating the economics of these systems. The MSBR program was discontinued in 1974 in favor of the sodium fast-breeder reactor design, and work on molten salt reactors essentially stopped for several decades.

However, these three programs—ANP, MSRE, and MSBR—generated much of the existing data for fluoride salts as well as fluoride salt reactors. The significant amount of research performed during these programs covered areas such as materials compatibility with the salts,⁷ salt physical properties,⁸⁻¹⁰ heat transfer characteristics,¹¹ neutronics behavior,¹² component development,¹³ salt purification and handling techniques,¹⁴ and salt eutectic characterization,¹⁵ among many others. Hundreds of papers and reports were generated during the course of these programs; the ones previously cited are only a few examples but should give readers an entrance point into this literature. A partial list with links to ORNL reports on the subject can be found in reference 16.

After a long hiatus, interest in fluoride salts as a reactor fuel and coolant was renewed in 2002 when the Generation IV reactor program^{17,18} selected the molten salt concept as one of the six reactor types to be investigated. Initially, the molten salt portion of that program focused on traditional liquid salt fuel concepts using either uranium or thorium fuel. However, shortly after the Gen IV program began, a second concept emerged that used fluoride salt as coolant but combined it with a solid fuel.¹⁹ This configuration is called the advanced high-temperature reactor (AHTR) or the fluoride salt-cooled high-temperature reactor (FHR). Other Gen IV concepts, for instance some configurations of the very-high-temperature reactor, a gas cooled concept, also use liquid salts as the heat transfer medium in an intermediate cooling loop because of their attractive heat transfer properties.

France and Euratom, within the Gen IV International Forum, have been working on the liquid salt-fueled reactor concept focusing on a molten salt fast reactor design.^{20,21} The FHR design is primarily being pursued in the United States by ORNL,²²⁻²⁴ which is developing several FHR concepts, and by a university consortium led by the Massachusetts Institute of Technology; the University of California, Berkeley; and the University of Wisconsin,^{25,26} which is developing a concept that uses solid fuel imbedded in graphite pebbles, the pebble bed-AHTR (PB-AHTR).

China has a very active liquid salt reactor development program,²⁷ with multiple experimental efforts designed to culminate in a test reactor using a pebble bed fuel design to be built by about 2017. They also are developing a molten-salt-fueled reactor design that will be built on information gathered with the test reactor. The Czech Republic is also involved in fluoride salt experimentation²⁸ and is planning to perform neutronics testing using salt (FLiBe) that was originally used in MSRE. India is also developing an FHR concept called the innovative high-temperature reactor²⁹ that uses a pebble bed core design. Russia also made a significant effort during the 1970s at the Kurchatov Institute in Moscow by studying a variety of aspects of molten salt coolant, including several different reactor design options and optimization studies, as well as materials development and compatibility testing programs.³⁰

Several small companies have been formed recently that are proponents of the molten salt reactor concept. Companies such as Terrestrial Energy,³¹ Havelide Systems,³² Flibe Energy,³³

Transatomic Power,³⁴ and ThorCon³⁵ have been formed, some promoting specific molten salt reactor concepts, others promoting the concept in general or specific aspects of molten salt reactors.

Even during the early years, as molten salt fission reactors were being developed, fluoride salts were also proposed as potential coolants for blanket modules in fusion reactor designs.^{36,37} A fusion reactor blanket, no matter what type of fusion reactor, generally has three requirements: (1) remove heat generated by the fusion reaction, (2) generate tritium to replace that used in the fusion reaction, and (3) shield structural materials from the neutron field generated by the plasma. Fluoride salts are very attractive candidates to meet the first two of these requirements. Liquid fluoride salts have good thermal transport properties, and therefore good heat transfer characteristics, and can effectively fulfill the heat-removal requirement. The second requirement is often met by introducing lithium into the blanket design, with tritium produced by neutron capture. To improve tritium production, beryllium is also often introduced in those designs. FLiBe salt is therefore often proposed as a potential blanket coolant, although other salts might also be attractive³⁶ for tritium production. Although the salt itself is not a very good neutron absorber, it is very stable in a neutron field and is an effective coolant of shield components.

Various designs of liquid-salt-based tritium breeding blankets have been proposed. Some proposed designs use the salt only for breeding,³⁸ and some use the salt both to breed tritium and as a high-temperature heat transfer medium to remove blanket heat for power production.³⁹ Conventional fluoride salt breeder blanket designs use a circulating fluoride salt inside a breeding blanket structure. For the two fluid concepts, the salt is used only for tritium breeding and helium is often proposed for removing most of the plasma-generated heat.³⁸ However, some novel liquid salt blanket designs have been proposed that use a liquid fluoride salt “waterfall” facing the plasma.⁴⁰ In this concept the liquid actually forms the plasma-facing wall and is used to absorb first wall surface heating. Another concept proposed by Lawrence Livermore National Laboratory dissolves thorium in the breeding salt to produce ²³³U as well as tritium.^{41,42} The ²³³U would be used to fuel the fission reactor fleet and would provide an additional revenue stream for the fusion reactor.

Fluoride salts have also been proposed as thermal storage media, making use of the salt heat of fusion to provide a low mass/volume storage media. Misra and Whittenberger⁴³ have examined a variety of fluoride salt eutectics and congruently melting fluoride salts to determine their usefulness as a storage medium for solar space power applications. Their study looked at a variety of fluoride salts with melt temperatures between 973 and 1400 K and heat of fusion between 0.44 and 1.08 kJ/g. Fluoride salts have also been proposed as storage media using only their sensible heats. The small AHTR²⁴ (SMAHTR) reactor concept used a “salt vault” to couple multiple reactors. The proposed storage used the sensible heat of either liquid FLiNaK or NaF-NaBF₄ salts operating between 500 and 600°C to supply either process heat or heat for a power conversion system from multiple FHR-type reactors.

The renewed interest in fluoride salts for a wide variety of high-temperature energy applications implies that there will be a need to develop and adapt modern measurement techniques for this heat transfer medium. The material presented in this paper is intended as a first step in examining measurement techniques that have been developed since the ANP/MSRE programs were abandoned and where much of the research on fluoride salts was performed. The experimental apparatus discussed is intended to provide a relatively inexpensive and versatile platform for making several fluid and heat transfer measurements in a liquid fluoride salt and for investigating potential measurement techniques that could be used as the previously discussed programs progress. The apparatus has been used to test instrumentation and measurement techniques that are used in conventional heat transfer systems but have not been applied to high-temperature fluoride salts. Other than a few materials compatibility studies⁴⁴ and some fluoride salt properties measurements^{45, 46} and assessments,^{47,48} little thermal/fluid experimental work has been performed on fluoride salts since those early investigations.

1.2 EXPERIMENT DESIGN

The experiment uses ~4 L of FLiNaK salt. A three-dimensional schematic of the experimental cell is shown in Fig. 1. It shows the cell inserted into an electrically heated furnace used to maintain cell temperatures. A nickel crucible holds the liquid salt and is located inside an outer stainless steel vessel that is used to maintain the correct inert atmosphere. An ultrapure argon cover gas is used over the salt, and a small argon flow rate is maintained to continuously sweep that area. A heater located in the center of the cell is used to induce natural circulation in the liquid salt and maintain a hot-to-cold surface temperature difference. A three-junction thermocouple probe allows salt temperature measurement at three axial locations.

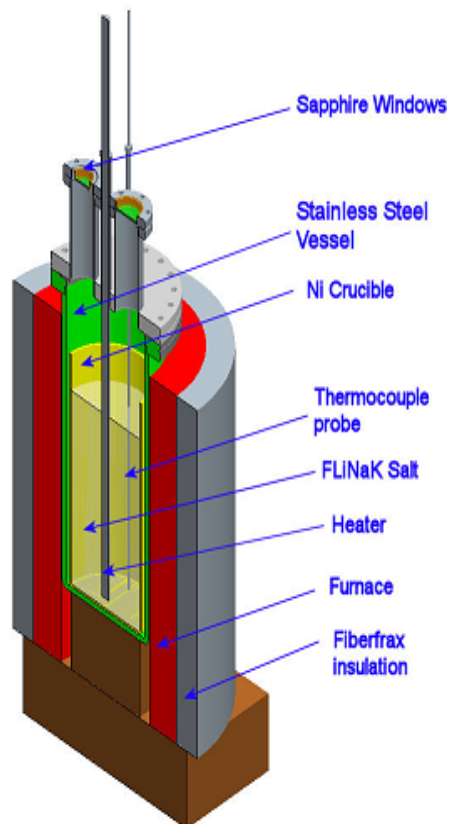


Fig. 1. Schematic of liquid salt cell.

Four thermocouples located internal to the heater system are used to measure heater surface temperature during operation. The heater and thermocouple probe were fabricated by Delta-M Corporation using nickel as the outer sheath material. Temperature measurement errors were estimated from the thermocouple calibration curves to be 0.55°C (a 1σ value). The heater is powered using a BK Precision VSP-12010, 0-120V, 0-10A dc power supply. Error in the measured power was a maximum of 2.5%. The flange at the top of the cell includes two sapphire viewports that allow visualization of the salt and the use of other optical measurement techniques including infrared (IR) imaging and laser Doppler velocimetry (LDV). Some of the cell's components are shown in the following pictures.

The upper flange (used in first series of testing) is made of stainless steel and is shown in Fig. 2. The two large ports visible in the picture allow viewing of the salt through sapphire windows during operation. The center tube (yellow cap) is where the heater element is inserted. The tube to the left (with two compression fitting caps) allows insertion of two thermocouples

used to measure vapor temperature in the cell. The tube with the green cap is where the three-junction thermocouple probe is inserted to measure salt temperatures. The Y-shaped tubing to the right is used to keep an argon purge gas in the cell. Argon overpressure in the cell is maintained at a few pounds per square inch to ensure that no air can ever enter the cell. The purge tubes are bent upward inside the window ports to maintain a purge gas flow over the inner window surface. (The sapphire windows have not been installed in the device shown in Fig. 2.) One of the two red-capped tubes is used to exhaust the argon purge gas, and the second is a spare port.

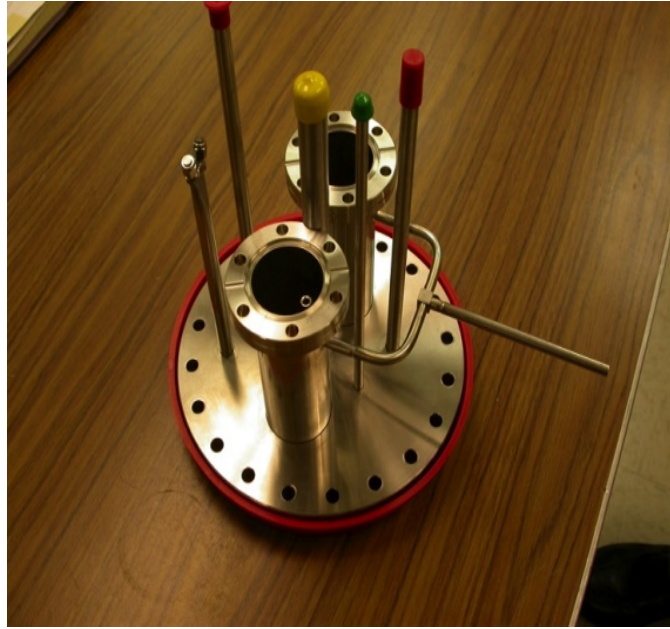


Fig. 2. Upper flange of cell.

Later in the testing program, a second upper flange was constructed that allowed removal of corrosion/compatibility test specimens while the salt was still at temperature and molten. It included all of the features of the first flange but added a 76 mm gate valve that allowed specimens to be removed from the melt while maintaining an inert argon cover over the specimens and melt. Figure 3 is a drawing of the second flange design. The test samples were submersed in the salt using a rod that extended through the top of the sample antechamber, with the gate valve open. When samples were to be removed from the melt, the samples were lifted from the melt using the holder rod until they were above the gate valve and in the antechamber. The gate valve was then closed. A glove bag was placed over the glove bag port and the glove bag evacuated. The blind flange that closed the glove bag port (not shown in Fig. 3) was removed exposing the samples to the glove bag. The samples were removed from the antechamber, and the glove bag port was resealed with the port flange. The glove bag was then isolated and removed from the glove bag port along with the test samples. Before opening the gate valve, the antechamber was evacuated and refilled with argon gas and the crucible and antechamber pressures equalized. The gate valve was then opened, and the remaining samples were returned to the melt. A picture of the modified flange is shown in Fig. 4.

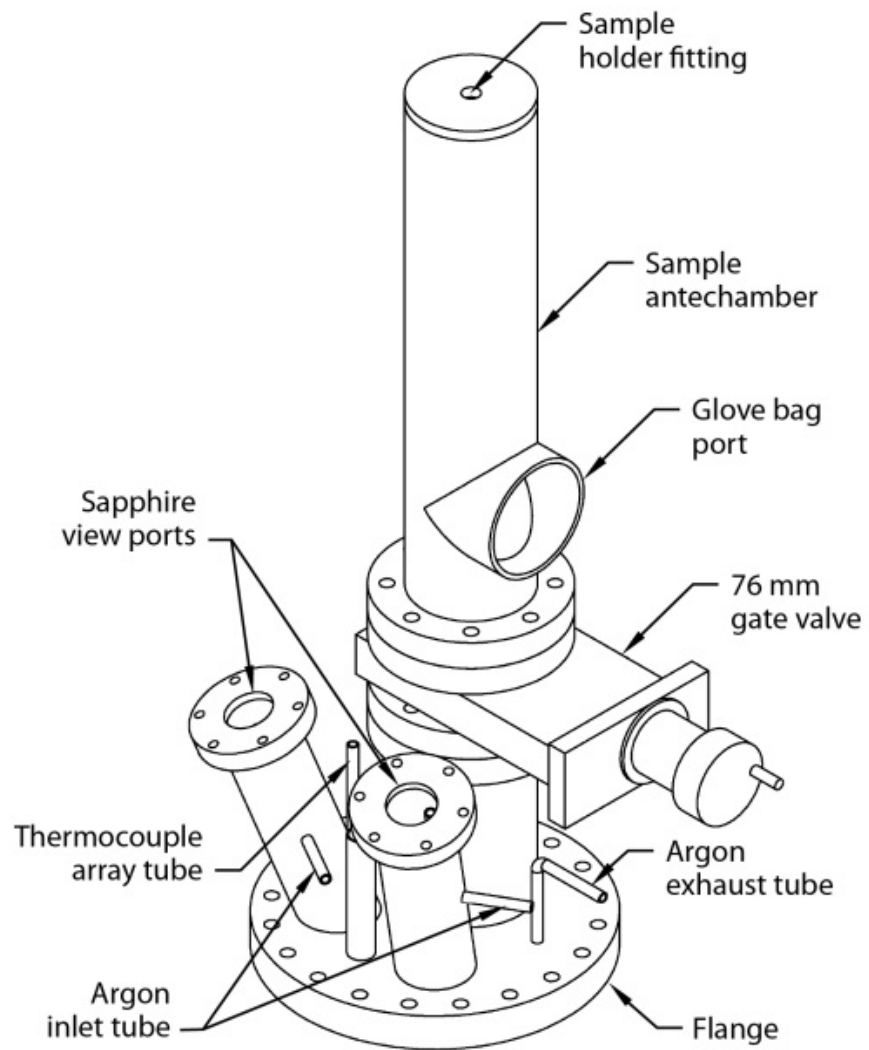


Fig. 3. Improved top flange.



Fig. 4. Modified top flange showing 76 mm gate valve.

The nickel crucible that holds the salt is shown in Fig. 5. Tabs on the outer surface located at the top and bottom of the crucible center are on the outer vessel. The outer vessel with the crucible inserted is shown in Fig. 6. The upper flange assembly, including the windows, is shown temporarily assembled in the vessel in Fig. 7, and the assembly is shown inserted in the furnace in Fig. 8.



Fig. 5. Nickel crucible used to contain liquid salt.



Fig. 6. Outer vessel with crucible inside.



Fig. 7. Top flange temporarily assembled to vessel.



Fig. 8. Assembly inserted in furnace.

The dimensions of the cell are shown in Fig. 9. The nickel crucible is 13.3 cm in diameter and 31.2 cm in height. During an experiment, the salt level is within ~2.5 cm of the top of the crucible. The furnace surrounding the outer vessel was manufactured by Watlow and has three vertical heating zones that allow higher heating levels at the top of the crucible to prevent salt from deforming the crucible during the melting process. The furnace heaters are controlled using Omega proportional-integral-derivative power controllers. The outer surface of the furnace is insulated with Fiberfrax insulation. Approximately 5 cm of insulation is extended to cover the top flange of the vessel. The vessel and furnace both sit on firebrick to provide insulation and to position them vertically.

Optical measurement techniques have advanced significantly over the last 20 to 30 years, and because of fluoride salt optical properties, as well as low-pressure operation of fluoride salt systems, these techniques could provide unique measurement opportunities. A recent evaluation of optical measurements as applied to advanced small modular reactors specifically identified IR imaging, LDV measurements, and visual observations as potential measurement methods that could be used with both MSR and FHR reactor designs.⁴⁹ The discussion and experimentation presented here is an initial attempt at examining the difficulties and usefulness of these techniques applied to high-temperature operation of fluoride salt systems.

1.3 VISUALIZATION

To observe the salt, a high-intensity fiber-optic light source (Cuda Products Corporation Model I-150) and lens system are used to illuminate the cell through one of the sapphire windows. A Toshiba Teli Corporation video system equipped with a Kowa Company, Ltd., 18–108 mm macro lens is mounted above the other port to observe the salt during testing.

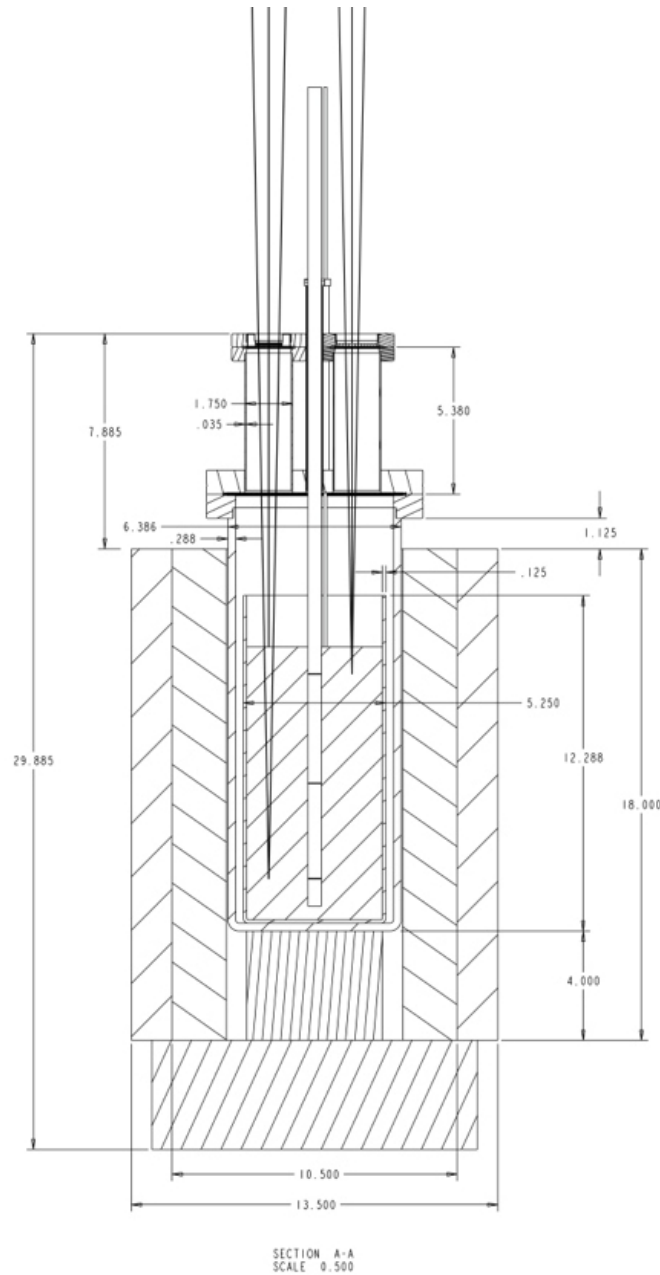


Fig. 9. Salt cell dimensions.

Still photography is also used to capture images of the salt and internal components. An example is shown in Fig. 10. The heater can be seen at the left of the photo. The salt is completely clear. The “spots” seen in the figure are actually on the bottom of the 31 cm tall nickel crucible and appear to be regions in which the reflectivity changes in the bottom of the crucible, perhaps because of the welding process used in fabrication. The three-thermocouple probe is also clearly visible in the figure. The liquid salt surface level can be seen as the dark “ring” around the heater. There is an obvious meniscus around the heater and thermocouple probe. The change in angle at which the light penetrates the liquid causes this shadowed region on the heater and the thermocouple probe to “disappear” around the salt surface in the picture. It becomes “hidden” in the neighborhood of the meniscus as the curvature of the liquid salt defines zones that cannot be imaged.

Figure 10 also shows a rendering of the view in the picture for clarity. It was found during testing that providing the light source through one window and viewing through the second window provided the best illumination. Sometimes the light source had to be adjusted so that shadows caused by the structure of the top flange did not darken the picture area of interest.

During testing the experiment operated continuously with salt melted for ~1 month at several salt temperature levels. The windows remained clear (or nearly so) for all but operation at 700°C. Operation at this temperature tended to cause salt condensation on the window surface, clouding visibility through the window. When the system was disassembled after testing, the condensate was found to be a very fine powder consisting of fluorides of sodium, potassium, and lithium that could be easily removed by lightly brushing with a paper towel. Figure 11 shows a picture of one of the clouded windows during testing. To use optical techniques, the windows will need to remain clear. The windows might need to be operated at higher temperatures, or cleaned in some way (mechanically high velocity gas, etc.), to prevent fogging.

1.4 IR PHOTOGRAPHY

A FLIR Indigo Phoenix mid-wave IR camera was used to evaluate the utility of using IR photography or videography to measure temperatures of articles submerged in the salt. The salt itself was at a temperature of 700°C; however, the heater provided temperature differentials (heater to salt) of up to 30°C. The IR camera was focused on the heater element operating at about 300 W with heater thermocouples reading between 20 to 30°C higher than the surrounding salt temperatures.

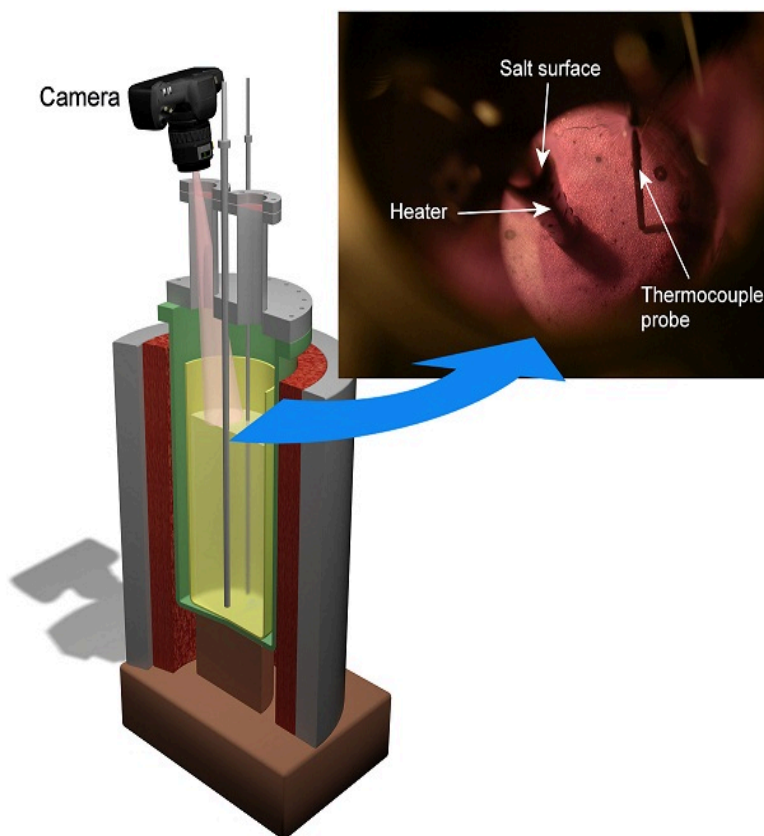


Fig. 10. Photo of salt through sapphire window.



Fig. 11. Sapphire window showing “fogging” after 1 month of testing.

Figure 12 is a plot of sapphire transparency versus wavelength and indicates that transparency is limited above a wavelength of about $4\ \mu\text{m}$. The IR camera operated in a wavelength range of ~ 3 to $5\ \mu\text{m}$, so it was recognized that the resolution would be affected; however, this test was conducted to determine whether a temperature difference could be detected even with this limitation.

Figure 13 shows the results of one test. The still image shown is one frame of a video taken with the camera looking down through the sapphire window. The heater element can be seen as the lighter area ranging from the lower left to the upper right of the window. As shown in this picture, the camera does detect temperature differences in the heater element, but there is a significant lack of resolution. It was thought that with the addition of filters on the camera, this resolution could be significantly improved; however, the testing had to be terminated before the effect of selective filtering could be evaluated. Other salt-compatible window material might be available that has better transparency in the IR region, but this project was not able to evaluate that possibility. The measurements taken here were only the first step in evaluating this measurement technique, but they were sufficiently successful to warrant additional investigation.

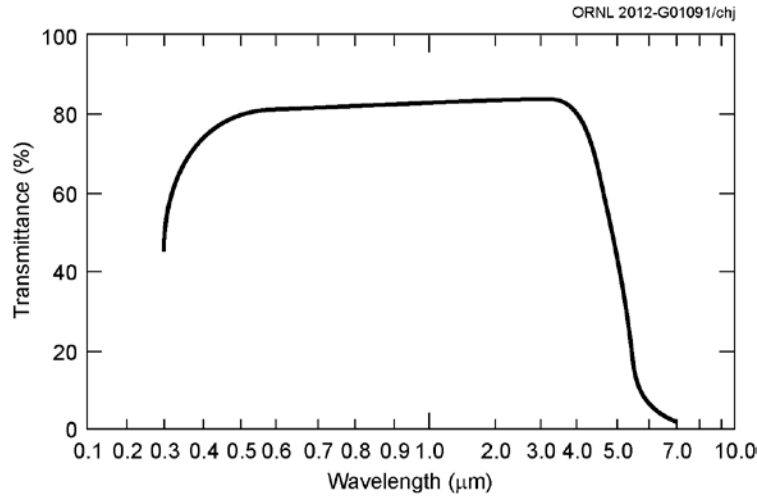


Fig. 12. Transmittance of sapphire window.

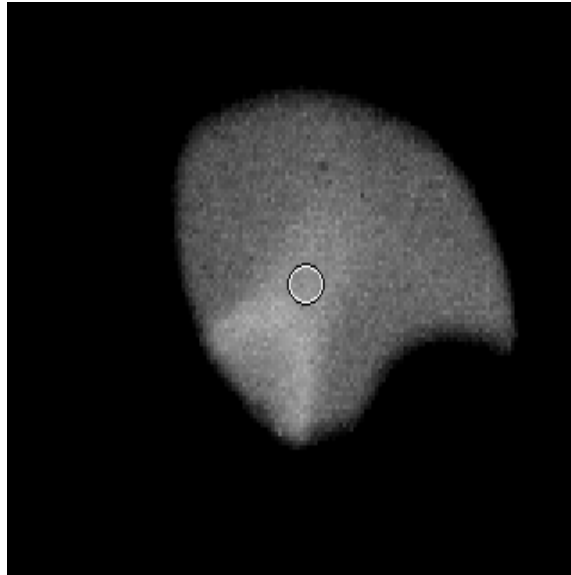


Fig. 13. IR image of heater immersed in salt.

1.5 LASER DOPPLER VELOCIMETRY

A TSI, two-dimensional LDV with an IFA750 signal processor operating at wavelengths of 488 and 514.5 nm was used to examine velocities within the salt cell. Predictions using computational fluid dynamics (CFD) calculations indicated that velocities on the order of 3 cm/s could be expected. This velocity is in the lower range of what can be detected using the LDV system, but measurements should still be possible.

The TSI LDV system uses an 83 mm, two-component fiber-optic probe to position the two laser beams. A 900 mm focal length lens was purchased for this system to allow the head to be located at a distance from the sapphire window that would allow both beams to pass through the window and still cross within the region of salt that was of interest. Because of the window orientation at the top of the melt, the velocity directions that could be measured were in the r - ϕ plane of the melt, as opposed to the z direction (vertical), which is the major flow direction. To

evaluate the technique, for most of the testing the beam intersection was located at either the top or bottom of the melt (where radial and azimuthal velocities would be highest).

Tests were initially conducted without any seeding of the salt melt. These tests produced no statistically significant velocity results because of the purity of the salt and lack of seed material within the melt. A seed material was then introduced into the melt through one of the spare ports in the top flange of the apparatus. Boron nitride (BN) powder was used as seed material because of its compatibility with the salt and because the density of the BN is very similar to that of the FLiNaK salt. When the BN powder was introduced, it was noted through the viewing port that the powder tended to clump together, some of it lying on the top of the melt and other portions of the material sinking to the bottom of the melt. It is not known at this point exactly why the seed material behaved in this way. Perhaps it did so because of wettability issues and/or gases entrapped in the BN particles and clumps. LDV tests were still conducted with the hope that some of the particles would be entrained in the flow and that a sufficient amount of seed material would be in the bulk of the melt. Unfortunately, the research team could not get any statistically significant velocity measurements, and additional work is needed to develop an effective seed technique. Perhaps mechanical mixing of the melted salt and BN would provide sufficient seed material density in the salt, or experiments with higher velocities might promote seed/salt mixing. The testing had to be terminated before any of these techniques could be investigated. Because it was recognized that introduction of BN would contaminate the salt, these tests were chronologically the last tests conducted with this salt batch.

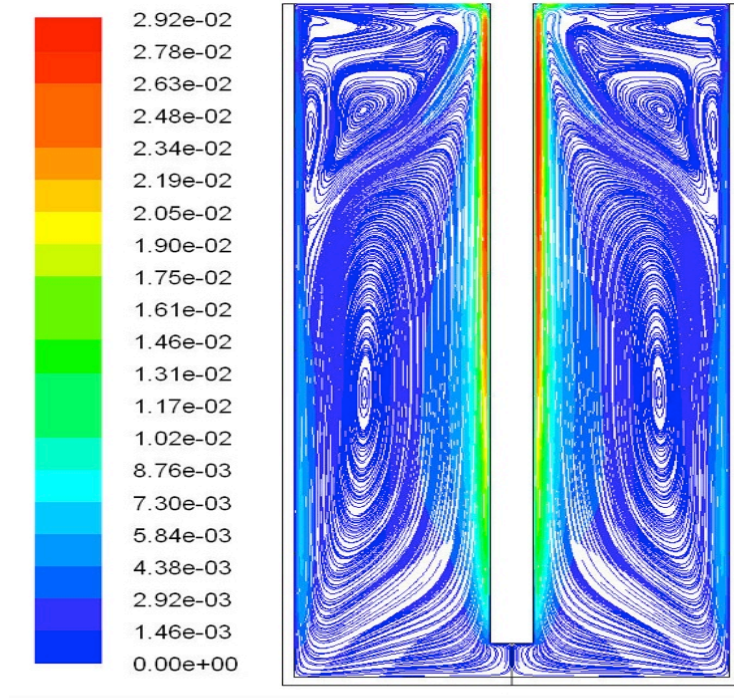
1.6 SALT VELOCITY CALCULATIONS

A series of calculations using the FLUENT CFD code were performed to examine the natural circulation and thermal behavior of the cell. Example results from these calculations are shown in Figs. 14 and 15. An axisymmetric geometry was chosen for this analysis. The heater is represented as the white rectangle in the center of each figure, while the crucible holding the salt is the white “outline” in each case. Only the region of the crucible containing salt was modeled. Figure 11 shows predicted velocity profiles inside the cell for 200 W of heater power. (Design heater power is 500 W.) The salt was maintained at a temperature of 700°C for this calculation (the maximum operating temperature that was used in the experiment). Fluid velocities near the heater were ~3 cm/s. This velocity level was also typical of the velocities developed in the harp-type corrosion experiments run with liquid salts in the past⁵⁰. A large, annular recirculation region over the major portion of the salt is noted in the Fig. 13, which is what is qualitatively expected. However, the convective boundary condition between the salt and argon cover gas imposed at the top of the salt causes a series of recirculation cells to form at the top of the melt.

Temperatures are shown in Fig. 15. The maximum temperature difference in this example is ~30 K (although temperature differentials as high as 100–150 K should be possible with the heater operating at maximum power). As expected, the highest temperatures surround the heater and are near the top of the heater element. The major portion of the salt remains at a lower temperature, however, because of the fluid motion. The hot salt flowing over the top of the heater section is swept across the salt surface and to the cold crucible wall, so a high-temperature region is also seen at the top of the melt.

These calculations were done in part to evaluate natural circulation heat transfer, but were done primarily to evaluate the cell concept for use in corrosion studies. Traditional harp-type natural circulation experiments⁵⁰ are typically used to establish temperature gradients between two materials using a natural convective flow. Harp experiments are D-shaped; one leg of the D is the hot (and heated) region, while the other leg is the cold (and cooled) region. A natural circulation flow is established in the D because of this temperature gradient. In the cell configuration, the heater acts as the hot region and the crucible wall as the cold region. With this configuration, the sheath could be fabricated from the material with corrosion characteristics of

interest, and the desired temperature differences could be established by the amount of power to the heater. A variety of corrosion studies could be easily performed using this geometry by simply changing the heater sheath rather than the entire harp loop. The calculations show that the natural circulation flows in the cell are very similar to those in a similar harp configuration, while temperature differences are also very similar, easily varied, and easily controlled. Ignatiev et al.⁵¹ performed corrosion testing using a cell-type geometry and natural circulation within the cell.



Pathlines Colored by Velocity Magnitude (m/s)

Fig. 14. Velocity path lines and magnitude as predicted by FLUENT CFD analysis.

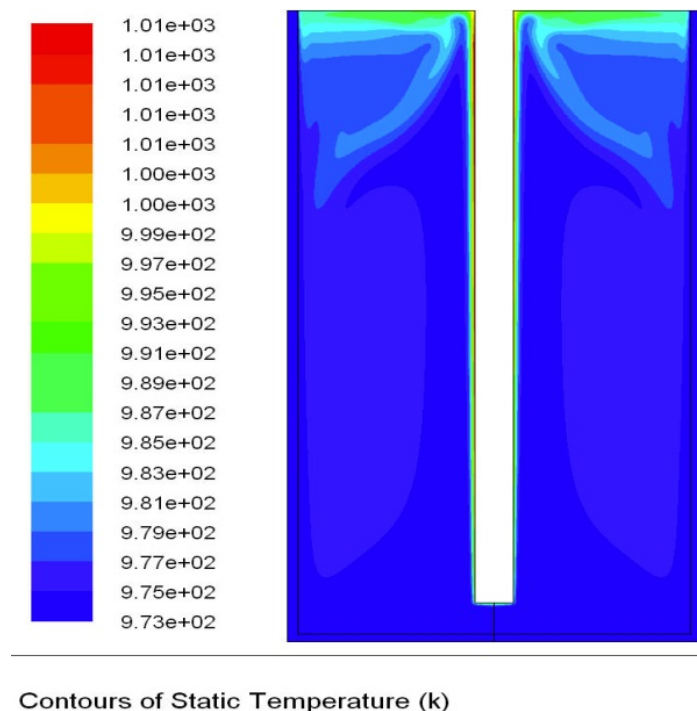


Fig. 15. Temperature profiles within the melt.

The experiment used separate specimen samples and an internal geometry that allowed heating of the salt from the outside of the cell at the bottom and cooling of the salt from the outside of the cell at the top of the experiment. The geometry proposed here is simpler, and the cell configuration, therefore, seems to be a good candidate for performing corrosion testing under temperature differentials and mild convective conditions.

1.7 NATURAL CIRCULATION HEAT TRANSFER DATA

A limited amount of heat transfer data is available for liquid fluoride salt systems. Less than 10 sets of experiments are available that characterize fluoride salt heat transfer, and the quality of the data and reported experimental detail varies greatly. The data were taken in the 1950s through 1970s. A summary of available FLiNaK forced convection heat transfer data has been presented by Ambrosek,⁵² who identified four data sources and tried to assimilate that data to develop generalized conclusions on FLiNaK heat transfer. A more general review of the state of technology for molten salt coolants, including heat transfer, was presented by Holcomb and Cetiner,⁵³ and two additional sources of fluoride salt (not FLiNaK) heat transfer data beyond that identified by Ambrosek were referenced. Not mentioned in any of these reports are data taken by Silverman et al.,¹¹ who performed heat transfer measurements in LiF-BeF₂-ThF₂-UF₄ and NaBF₄-NaF salts. All seven of the sets just mentioned were taken under forced convection conditions. The author is unaware of any natural circulation heat transfer data taken using fluoride salts. A review of fluoride salt heat temp experimentation and discussion of the data are given by Yoder.⁵⁴

A series of tests were run in the apparatus previously described with heater power and salt temperatures parametrically varied to determine the natural circulation heat transfer coefficients at the surface of the heater. Because there were heater failures, three heaters were used for this experimentation. The geometries used are presented in Figs. 16–18. Heaters 1 and 2 were separate heaters. However, after it failed, heater 2 was repaired to make heater 3. To repair the heater, the bottom thermocouple had to be eliminated; therefore, heater 3 had no bottom

thermocouple. The thermocouple probe (see Fig. 17) was installed midway between the outside diameter of the heater element and the nickel liner inner wall and remained in the same location for the duration of testing.

To perform these tests, a steady overall salt temperature was established using the furnace system. The heater element power was then set at the desired level. The cell was allowed to stabilize until steady salt and heater temperatures were achieved. Both heater and salt temperature data were then taken, and heater voltage and current were recorded. In general, three overall salt temperatures were tested: 600, 650, and 700°C. Temperature and heater power data are shown in Table 1 for 11 separate tests, which represent data from all three heaters. Salt temperatures were taken using the thermocouple array, with thermocouple locations as indicated in Fig. 19. Heater thermocouple locations are indicated in Figs. 16–18 and depend on the specific heater used. A thermocouple was also placed in the argon cover gas above the salt melt as well as in the space (also filled with argon) between the nickel crucible and stainless steel outer vessel (vertical centerline of the melt). These measurements are also shown in Table 1.

Table 2 shows heat transfer coefficients on the heater surface calculated from the data. Heater power was calculated from current and voltage readings from the dc power supply. The local natural circulation heat transfer coefficient, h_{nc} , was calculated as follows:

$$h_{nc} = (q'' - q''_{rad}) / (T_h - T_s) ,$$

where

q'' = average heater heat flux: P/A_s ,

q''_{rad} = radiation correction,

P = heater power = Vi ,

A_s = heater surface area (based on heated length of heater),

i = current,

T_h = measured local heater temperature,

T_s = measured local salt temperature,

V = voltage.

A radiation correction q''_{rad} was calculated assuming grey body radiation between the heater element and crucible. Nickel emissivity was assumed to be 0.1, and the FLiNaK was assumed to be transparent. The latter assumption is an open question with fluoride salts, as very little absorptivity measurements have been taken using these salts. The radiation correction was less than 5% for all data points. In calculating the uncertainty in measured heat transfer coefficients, a 100% uncertainty was assumed in the radiation correction term.

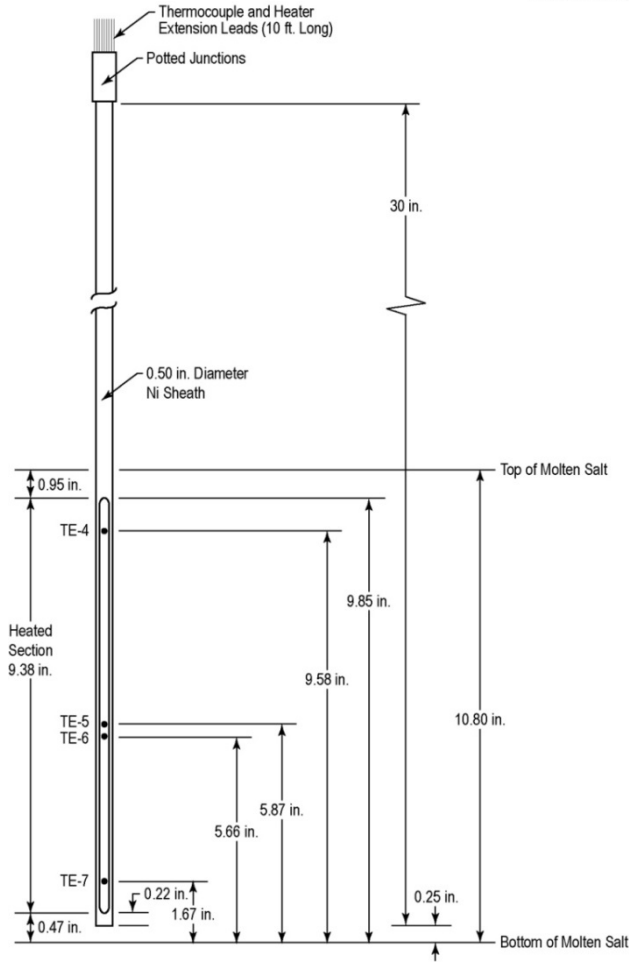


Fig. 16. Heater 1 thermocouple locations.

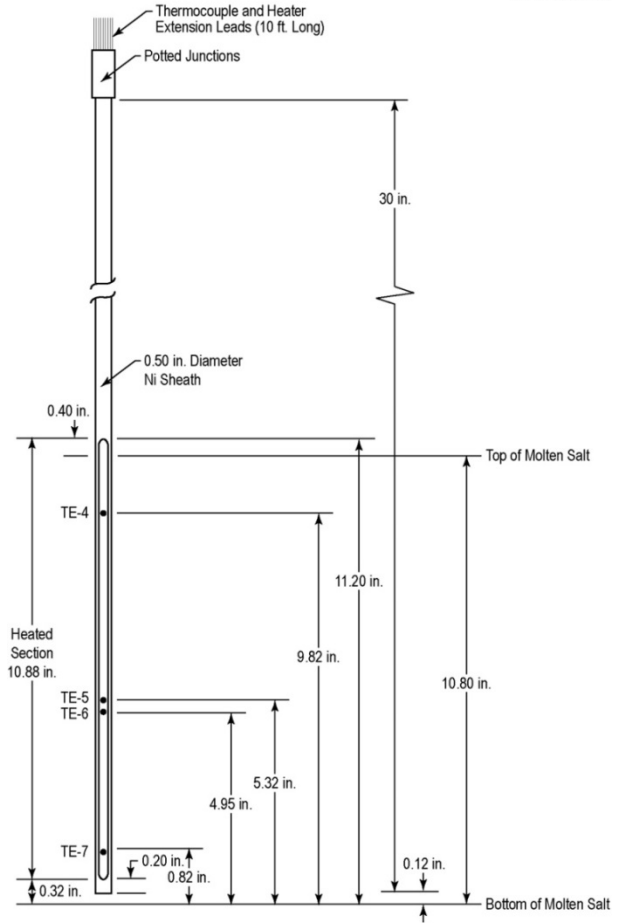


Fig. 17. Heater 2 thermocouple locations.

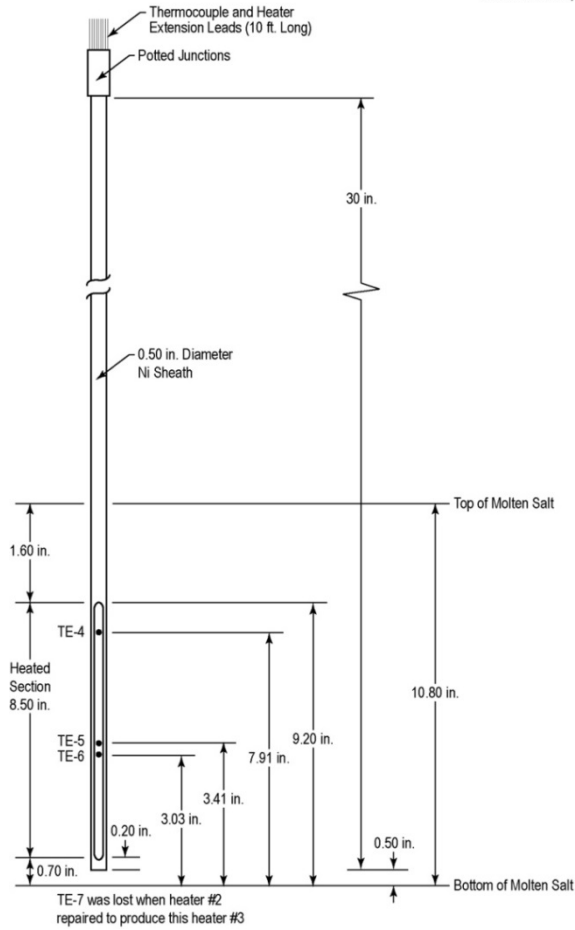


Fig. 18. Heater 3 thermocouple locations.

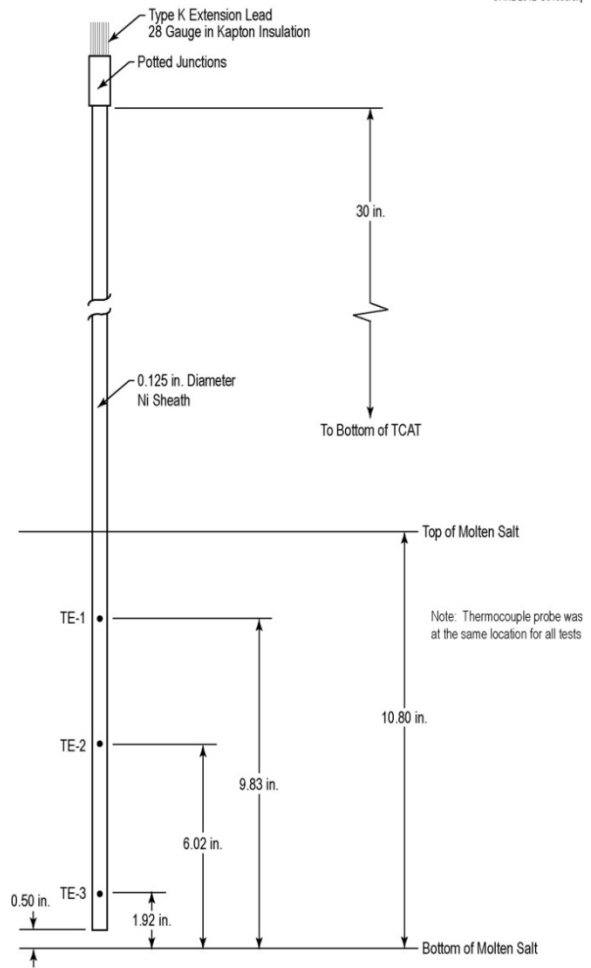


Fig. 19. Thermocouple probe thermocouple locations.

Table 1. Natural circulation heat transfer data from liquid salt cell testing

Test	Heater #	Salt temperature (°C)			Heater temperature (°C)				Argon cover gas temperature (°C)	Crucible gap temperature (°C)
		Top TE-1	Middle TE-2	Bottom TE-3	Top TE-4	Middle #1 TE-5	Middle #2 TE-6	Bottom TE-7		
1	1	563	561	561	596	600	600	590	447	568
2	3	609	608	608	647	644	642		487	617
3	3	610	609	609	647	646	644		493	617
4	2	567	565	565	601	598	597	586	455	571
5	2	603	597	594	654	646	645	623	478	583
6	2	634	625	617	699	688	687	652	510	594
7	2	611	610	610	644	641	642	631	505	623
8	2	640	635	634	690	684	683	665	526	632
9	2	639	635	633	690	685	684	667	521	632
10	3	610	609	609	648	645	644		498	621
11	2	603	597	594	654	647	645	623	479	583

Table 2. Calculated values of heat transfer coefficients

Test	Heater power (W)	Heat transfer coefficient, h_{nc} (W/m ² /°C)			
		Top	Middle #1	Middle #2	Bottom
1	213	674	566	576	775
2	208	634	677	700	
3	212	662	667	707	
4	210	559	577	588	879
5	369	658	680	696	1161
6	525	727	754	776	1360
7	212	586	624	610	919
8	364	658	671	686	1051
9	371	654	675	688	1011
10	210	634	678	699	
11	369	658	679	696	1165

In calculating T_s as used in the heat transfer coefficient, the local measured salt temperature was interpolated to the elevation corresponding to the heater temperature measurement elevation. The heater thermocouples were located directly inside the nickel heater sheath. The calculated temperature drop across the sheath was less than 0.1°C, so the measured heater temperature was assumed to be the heater outer wall temperature for the heat transfer coefficient calculation.

A plot of the heat transfer coefficient versus ($T_h - T_s$) is shown in Fig. 20. The data are plotted as a function of the heater thermocouple location. For instance, the green triangles are from the bottom heater thermocouple and tend to have higher heat transfer coefficients than the remainder of the data. Because the thermal boundary layer grows as $Z^{1/4}$ (for laminar flow) with the boundary layer thickness equal to 0 at the beginning of the heated length, the thermal resistance tends to be relatively lower (and heat transfer coefficients relatively higher) at the bottom of the heater. Error bars shown in Fig. 20 represent measurement errors.

For laminar natural convection flow in a vertical orientation, the Nusselt number, Nu , is proportional to the Grashof number, Gr , raised to the one-fourth power:

$$Nu \propto Gr_z^{1/4}$$

and for turbulent flow

$$Nu \propto Gr_z^{1/3},$$

where

- Nu = Nusselt number $h_{nc} z/k$,
- Gr_z = Grashof number $g\rho^2\beta z^3(T_h - T_s)/\mu^2$,
- h_{nc} = natural circulation heat transfer coefficient,
- k = salt thermal conductivity,
- g = acceleration of gravity (9.8 m/s²),
- ρ = salt density,
- β = salt thermal coefficient of volume expansion,
- z = distance from bottom of heater element,
- T_h = heater temperature,
- T_s = salt temperature,
- μ = salt dynamic viscosity.

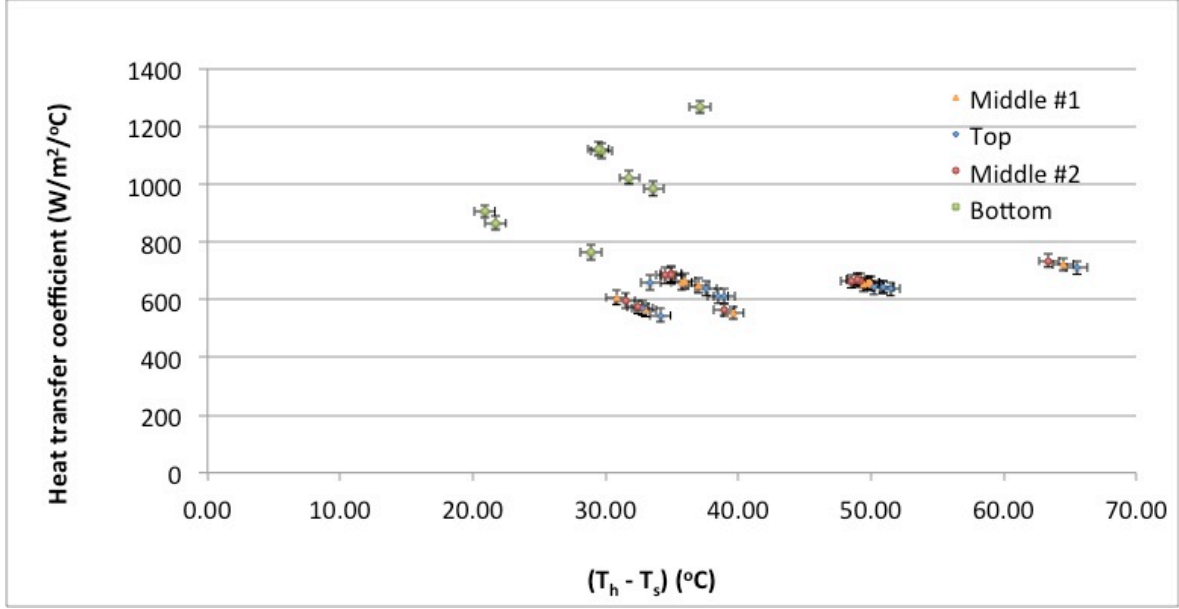


Fig. 20. Heat transfer coefficient data.

A typical laminar flow correlation for Nu for $10^4 < Gr_z Pr < 10^9$ is

$$Nu_l = 0.56 (Gr_z Pr)^{1/4}$$

and for turbulent flow for $10^9 < Gr_z Pr < 10^{12}$ is

$$Nu_t = 0.13 (Gr_z Pr)^{1/3} ,$$

where

Pr = Prandtl number $\mu C_p/k$,
 C_p = salt specific heat.

Both correlations, taken from Rohsenow and Choi,⁵⁵ were developed for flow over a vertical plate and are compared to the present data in Fig. 21. Error bars on the data reflect measurement error in heater power, heater temperature, and the radiation component as noted previously. In some cases (lower Nu values), the error bars are smaller than the symbol size and cannot be seen in the figure. The preceding laminar and turbulent equations are indicated in the figure as solid lines. The salt data compare very favorably to these traditional correlations. Also shown in Fig. 21 are best-fit equations to the data. These have slightly different leading coefficients and exponents on the GrPr parameter. Table 3 provides a comparison of these equations.

As Fig. 21 indicates, the data can be predicted reasonably well using conventional natural circulation correlations developed using other fluids.

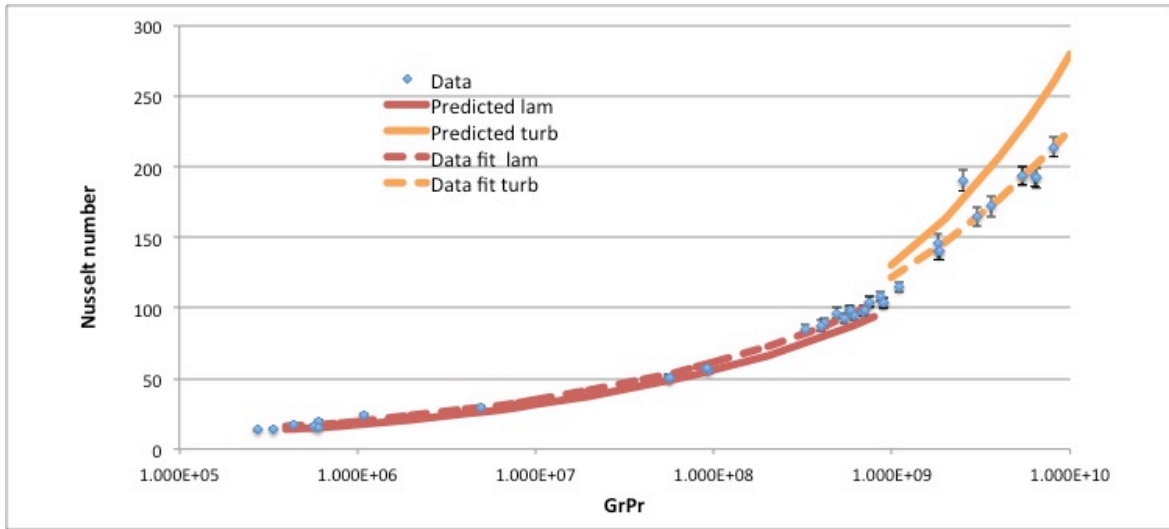


Fig. 21. Nusselt number data comparison.

Table 3. Comparison of Nu equations of the form $Nu = A(GrPr)^b$

Correlation	A	b	R ²
Ref 1 laminar	.56	.25	.997
Ref 1 turbulent	.13	.3333	.925
Data fit laminar	.665	.246	.997
Data fit turbulent	.438	.272	.927

2. CONCLUSIONS

A versatile experiment has been developed that allows a variety of testing to be performed using fluoride salt operating at up to 700°C. Experiments were performed to examine the use of LDV, IR videography, and visualization using standard videography through sapphire windows. Each of these techniques was successful except for the LDV, where seed material could not be adequately entrained in the salt. Natural circulation heat transfer testing was conducted using a 0.5 in. diameter instrumented heater element in the salt crucible. Results from this testing were consistent with conventional correlations for flow over a vertical plate.

3. REFERENCES

1. R. C. Brian and A. M. Weinberg, "Molten Fluorides as Power Reactor Fuels," *Nuclear Science and Engineering* **2**(6), 797-803 (1957).
2. E. S. Bettis et. al., "The Aircraft Reactor Experiment–Design and Construction," *Nuclear Science and Engineering* **2**(6), 804-825 (1957).
3. W. K. Ergen et. al., "The Aircraft Reactor Experiment–Physics," *Nuclear Science and Engineering* **2**(6), 826-840 (1957).
4. E. S. Bettis et. al., "The Aircraft Reactor Experiment–Operation," *Nuclear Science and Engineering* **2**(6), 841-853 (1957).
5. P. N. Haubenreich and J. R. Engel, "Experience with the Molten-Salt Reactor Experiment," *Nuclear Applications and Technology* **8**, 118-136 (1970).
6. E. S. Bettis, L. G. Alexander, and H. L. Watts, *Design Studies of a Molten-Salt Reactor Demonstration Plant*, ORNL-TM-3832, Oak Ridge National Laboratory, Oak Ridge, Tenn., 1972.
7. W. D. Manly et. al., *Aircraft Reactor Experiment–Metallurgical Aspects*, ORNL-2349, Oak Ridge National Laboratory, Oak Ridge, Tenn., 1957.
8. S. Cantor, *Density and Viscosity of Several Molten Fluoride Mixtures*, ORNL-TM-4308, Oak Ridge National Laboratory, Oak Ridge, Tenn., 1973.
9. S. Cantor et al., *Physical Properties of Molten-Salt Reactor Fuel, Coolant, and Flush Salts*, ORNL-TM-2316, Oak Ridge National Laboratory, Oak Ridge, Tenn., 1968.
10. W. D. Powers, S. I. Cohen, and N. D. Greene, "Physical Properties of Molten Reactor Fuels and Coolants," *Nuclear Science and Engineering* **17**(2), 200-211 (1963).
11. M. D. Silverman, W. R. Huntley, and H. E. Robertson, *Heat Transfer Measurements in a Forced Convection Loop with Two Molten-Fluoride Salts: LiF-BeF₂-ThF₂-UF₄ and Eutectic NaBF₄-NaF*, ORNL/TM-5335, Oak Ridge National Laboratory, Oak Ridge, Tenn., 1976.
12. R. S. Carlsmith, *Review of Molten Salt Reactor Physics Calculations*, ORNL-TM-1946, Oak Ridge National Laboratory, Oak Ridge, Tenn., 1967.
13. R. H. Guymon (ed.), *MSRE Systems and Components Performance*, ORNL-TM-3039, Oak Ridge National Laboratory, Oak Ridge, Tenn., 1973.
14. J. H. Shaffer, *Preparation and Handling of Salt Mixtures for the Molten Salt Reactor Experiment*, ORNL-4616, Oak Ridge National Laboratory, Oak Ridge, Tenn., 1971.
15. R. E. Thoma (editor), *Phase Diagrams of Nuclear Reactor Materials*, ORNL-2548, Oak Ridge National Laboratory, Oak Ridge, Tenn., 1959.
16. <http://moltensalt.org.s3-website-us-east-1.amazonaws.com/references/static/downloads/pdf/>
17. <http://www.gen-4.org/>
18. US DOE Nuclear Energy Research Advisory Committee and the Generation IV International Forum, *A Technology Roadmap for Generation IV Nuclear Energy Systems*, GIF-002-00, 2002.
19. C. W. Forsberg, P. F. Peterson, P. S. Pickard, "Molten-Salt-Cooled Advanced High-Temperature Reactor for Production of Hydrogen and Electricity," *Nuclear Technology* **144**, 289-302, 2003.
20. E. Merle-Lucotte et al., "Launching the Thorium Fuel Cycle with the Molten Salt Fast Reactor," proceedings of ICAAP '11, Nice, France, 2011.
21. C. Renault et al., "The Molten Salt Reactor (MSR) in Generation IV: Overview and Perspectives," GIV Symposium, Paris, France, September 9-10, 191-200, 2009.
22. D. Ingersoll et al., *Status of Pre-conceptual Design of the Advanced High-Temperature Reactor (AHTR)*, ORNL/TM-2004/104, Oak Ridge National Laboratory, Oak Ridge, Tenn., 2004.
23. V. Varma, et al., *AHTR Mechanical, Structural, and Neutronic Preconceptual Design*, ORNL/TM-2012/320, Oak Ridge National Laboratory, Oak Ridge, Tenn., 2012.
24. S. R. Greene, "SMAHTR–A Concept for a Small Advanced High Temperature Reactor," *Proceedings of HTR-10*, Prague, Czech Republic, 2010.
25. P. Bardet et al., "Design, Analysis and Development of the Modular PBAHTR," International

- Congress on Advances in Nuclear Power Plants (ICAPP 2009), Curran Associates, New York, 161–178, 2009.
26. http://web.mit.edu/nse/pdf/researchstaff/forsberg/FHR_Project_Presentation.pdf
 27. Z. Dai, “Current Status of the TMSR Project in China,” presented at the Shanghai Institute of Applied Physics, 2013.
 28. M. Hron, J. Kyncl, and M. Mikisek, “Reactor Physical Experimental Program EROS in the Frame of the Molten Salt Applying Reactor Concepts Development,” paper 9233, *Proceedings of ICAAP '09*, Tokyo, Japan, 2009.
 29. <http://moltensaltindia.org/wp-content/uploads/2013/02/Vijayan.pdf>
 30. V. M. Novikov, “The results of the Investigations of Russian Research Center “Kurchatov Institute” on Molten Salt Applications to Problems of Nuclear Energy Systems,” International Conference on Accelerator-Driven Transmutation Technologies and Applications, Vol. 346, 138-147, 1995.
 31. <http://www.terrestrialenergyinc.com/>
 32. <http://www.havelide.com/>
 33. <http://flibe-energy.com/>
 34. <http://transatomicpower.com/>
 35. J. Devanney, “ThorCon Summary Description. Version 0.60,” Martingale, Inc., Sisyphus Beach, Tavernier, Florida, 2012.
 36. W. R. Grimes and S. Cantor, *Molten Salts as Blanket Fluids in Controlled Fusion Reactors*, ORNL-TM-4047, Oak Ridge National Laboratory, Oak Ridge, Tenn., 1972.
 37. M. J. Saltmarsh, *Optimization of the Fission-Fusion Hybrid Concept*, ORNL/PPA-79/3, Oak Ridge National Laboratory, Oak Ridge, Tenn., 1979.
 38. M. Abdou et al., “U.S. Plans and Strategy for ITER Blanket Testing,” *Fusion Science and Technology* **47**, 475-487, 2005.
 39. D. K. Sze et al., “Conceptual Design of a Self-Cooled FLiBe Blanket,” *Fusion Technology* **10**(3), 624-632, 1986.
 40. M. A. Abdou et al., “Overview of fusion Blanket R&D in the US Over the Last Decade,” *Nuclear Engineering and Technology* **37**(5), 401-422 (2005).
 41. R. W. Moir et al., “Helium-Cooled, FLiBe Breeder, Beryllium Multiplier Blanket,” *Fusion Technology* **8**(1), Part 1, 133-148, 1985.
 42. R. W. Moir and J. D. Lee, “Helium-Cooled, FLiBe-Breeder, Beryllium-Multiplier Blanket for MINIMARS,” *Fusion Technology* **10**(3), Part 2(A), 619-623, 1986.
 43. A. K. Misra and J. D. Whittenberger, “Fluoride Salts and Container Materials for Thermal Energy Storage Applications in the temperature Range 973-1400K,” proceedings of Energy-New Frontiers, American Institute of Aeronautics and Astronautics, Philadelphia, (AIAA-87-9226) 188-201, 1987.
 44. L. C. Olson et al., “Materials Corrosion in Molten LiF-NaF-KF Salt,” *Journal of Fluorine Chemistry*, 130, 67-73, 2009.
 45. A. K. Misra, “Fluoride Salts as Phase Change Materials for Thermal Energy Storage in the Temperature Range 1000-1400K,” *Electrochemical Science and Technology* **135**(4), 850-854, 1988.
 46. A. K. Misra, “Densities of Some Molten Fluoride Salt Mixtures Suitable for Heat Storage in Space Power Applications,” *Electrochemical Science and Technology* **135**(11), 2780-2781, 1988.
 47. D. F. Williams, *Assessment of Candidate Molten Salt Coolants for the NGNP/NHI Heat-Transfer Loop*, ORNL/TM-2006/69, Oak Ridge National Laboratory, Oak Ridge, Tenn., 2006.
 48. D. F. Williams, “Revival of Halide Salts as High-Temperature Heat-Transfer Media: Key Technical and Scientific Issues,” *Electrochemical Society Transactions* **3**(35), 441-451, 2007.
 49. N. C. Anheier et al., *Technical Readiness and Gaps Analysis of Commercial Optical Materials and Measurement Systems for Advanced Small Modular Reactors*, PNNL-22622, Rev. 1, Pacific Northwest National Laboratory, Richland, Wash., 2013.
 50. J. Keiser et al., *Compatibility Studies of Potential Molten-Salt Breeder Reactor Materials in Molten Fluoride Salts*, ORNL-5873, Oak Ridge National Laboratory, Oak Ridge, Tenn., 1977.

51. V. Ignatiev et al., "Experience with Alloys Compatibility with Fuel and Coolant Salts and Their Application to Molten Salt Actinide Recycler & Transmuter," Proceedings of ICAPP '06, Reno, Nev., paper 6002, 2006.
52. J. Ambrosek et al., "Current Status of Knowledge of the Fluoride Salt (FLiNaK) Heat Transfer," *Nuclear Technology* **165**, 166-173, 2009.
53. D. Holcomb and M. Cetiner, *An Overview of Liquid-Fluoride-Salt Heat Transport Systems*, ORNL/TM-2010/156, Oak Ridge National Laboratory, Oak Ridge, Tenn., 2010.
54. G. Yoder, "Examination of Liquid Fluoride Salt Heat Transfer," Proceedings of ICAPP 2014, Charlotte, N.C., 2014.
55. W. M. Rohsenow and H. Choi, *Heat, Mass, and Momentum Transfer*, Prentice-Hall, Englewood Cliffs, N.J., 1961.